



Experiments Division

ALBA Project Document No:

EDMS Document No.

Created: 1/9/2006

Pages: 20

EXD-BL290P-GD-0001

Modified: 18/4/2007

Rev. No.: 3

*Conceptual Design Report
of the
Soft X-Ray Magnetic Circular Dichroism (XMCD) beamline
at the
ALBA Synchrotron Radiation Facility*

Prepared by:

**Franziskus Heigl
Alessandro Barla**

Checked by:

Approved by:

Distribution List

Contents

OVERVIEW	3
1 SOURCE	3
2 OPTICAL LAYOUT OF THE BEAMLIN.....	6
3 THE PRE-OPTICS SECTION	7
4 THE MONOCHROMATOR SECTION	8
5 THE REFOCUSING SECTION	13
6 THE EXPERIMENTAL SECTION	14
7 POWER LOAD ON THE OPTICAL ELEMENTS	14
8 DIAGNOSTICS SYSTEM.....	17
REFERENCES.....	19

Overview

CELLS is a consortium created to construct and exploit the ALBA synchrotron facility to generate x-rays for basic and applied research. The facility, which will be located near Barcelona, will include a 3-GeV, low-emittance storage ring able to run in top-up mode, which will feed an intense photon beam to a number of beamlines. These are placed tangentially to the storage ring and hold the experimental facilities. The XMCD-beamline is one of the beamlines to be implemented in the first phase of the ALBA project. It is designed for spectroscopies based upon soft x-ray absorption and scattering, and it will be equipped with two UHV compatible end stations. Both techniques will use monochromatized soft x-rays generated by an undulator with tunable linear and circular/elliptical polarization.

1 Source

The source is a PPM (Pure Permanent Magnet) APPLE II helical undulator, inserted in the center of one of the medium straight sections of the ALBA storage ring. This type of undulator is capable of delivering linearly polarized light, in all the directions, as well as circularly polarized light (left-handed or right-handed). The minimum magnetic gap of the undulator is limited to 15.5mm for homogeneity reasons (see Table 1). The total magnetic forces are limited to 20 kN. The undulator has 22 periods of 7.1cm length each, which results in a total length of 156.2cm. The specified motor speed for the phase change mechanism is 1mm/s, so the device is able to change between left and right circular polarization in about 31s. Details of the source design can be found in Ref. [1].

Table 1: Parameters of the HU71 APPLE II undulator.

Parameter	Value		
Type of ID	PPM Apple II		
Period (mm)	71.0		
Number of Periods	22		
Magnetic gap (mm)	15.5 – 90.0		
Magnetic length (mm)	1562		
Polarization modes	Circular/linear 0-90		
Polarization	Horiz.	Vert.	Circular
B_x (T)	0	0.71	0.57
B_y (T)	0.93	0	0.57
K_x	0	4.73	3.78
K_y	6.19	0	3.78
Lowest tunable energy (eV)	59	98	78
Max. Flux (Ph/s/1%BW@400mA)	$6 \cdot 10^{14}$	$6 \cdot 10^{14}$	$1.2 \cdot 10^{15}$

The storage ring is planned to be operated at a nominal current of 250mA (while the maximum possible is 400mA). The tuning curves of the flux delivered by the HU71 at 400mA ring current (flux at tuned energy) is shown

in Fig.1 for horizontal and circular polarization. Note that the 1st harmonic (C1) in the central emittance cone (100% circular polarization) significantly decreases in flux beyond $\sim 1\text{keV}$. At higher energies only mixed polarization states are available (e.g. 95% circular). The power delivered to the beamline may also impose the necessity of limiting the acceptance of the beamline to less than the central cone. This may reduce the flux at the central cone at the low energy end.

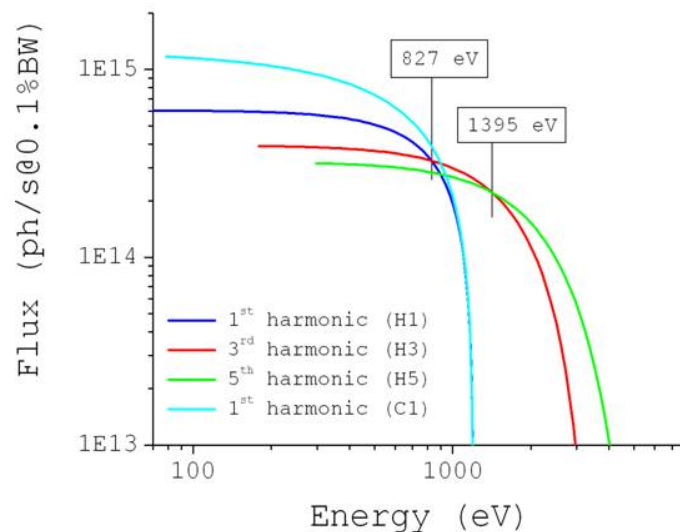


Figure 1: Flux emitted in central cone at tuned energy. Horizontal in 1st, 3rd, and 5th order and circular in 1st order are represented [2].

The horizontal source size is more or less constant over the whole energy range, because it is limited by the size of the electron beam. The vertical source size is mostly diffraction limited and changes from $\sim 70\mu\text{m}$ to $\sim 10\mu\text{m}$ towards the high energy end. The source divergence in the horizontal plane is diffraction limited only at low energies, whereas in the vertical plane the source divergence is diffraction limited over the whole energy range ($\sim 140\mu\text{rad}$ to $\sim 10\mu\text{rad}$). The spot size and divergence of the emitted photon beam are plotted in Fig.2.

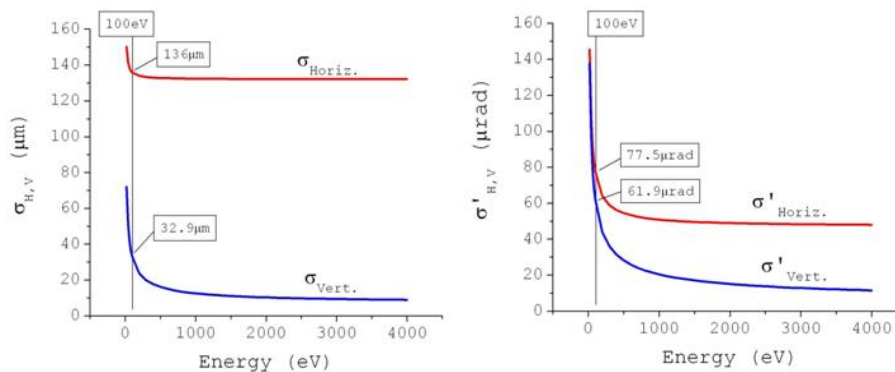


Figure 2. Spot size and beam divergence of the source. Red and blue refer to horizontal and vertical dimension respectively.

The shape of the characteristic angular power distribution depends on the polarization. In linear horizontal and vertical polarization the emission profile is a flat cone which is oriented accordingly. In circular polarization the power is distributed in a ring whose radius is determined by the K_x and K_y parameters (~ 0.5 mrad for minimum gap). In the region of interest (about ± 0.2 mrad), which corresponds to the angular spread of the first harmonic, most of the power can be removed by the white beam slits.

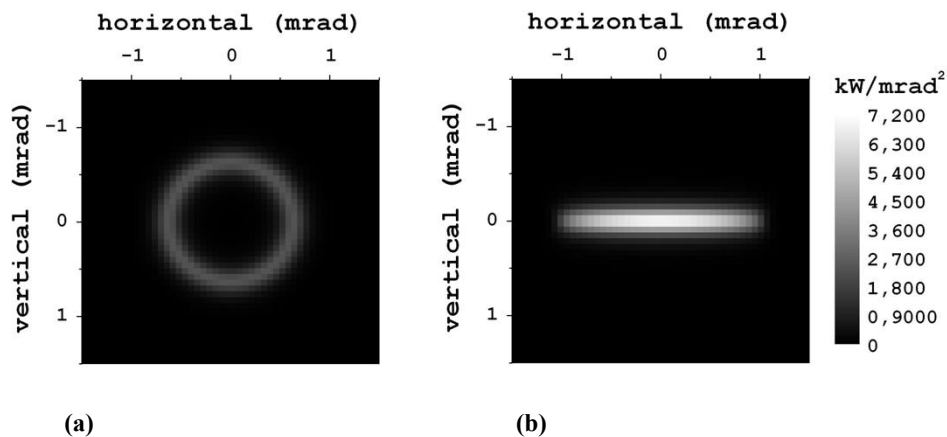


Figure 3: Emitted power from the source. Circular (a) and linear-horizontal (b) polarization at minimum gap (15.5mm).

The angular power distribution of circular and horizontal polarization at the smallest gap is shown in Fig.3. The angular power distribution along the symmetry axis at the lowest tuned energy is shown in Fig.4. The maximum power density which is used for estimating the power load on the optical elements is obtained in linear-horizontal polarization (cf. Table 2).

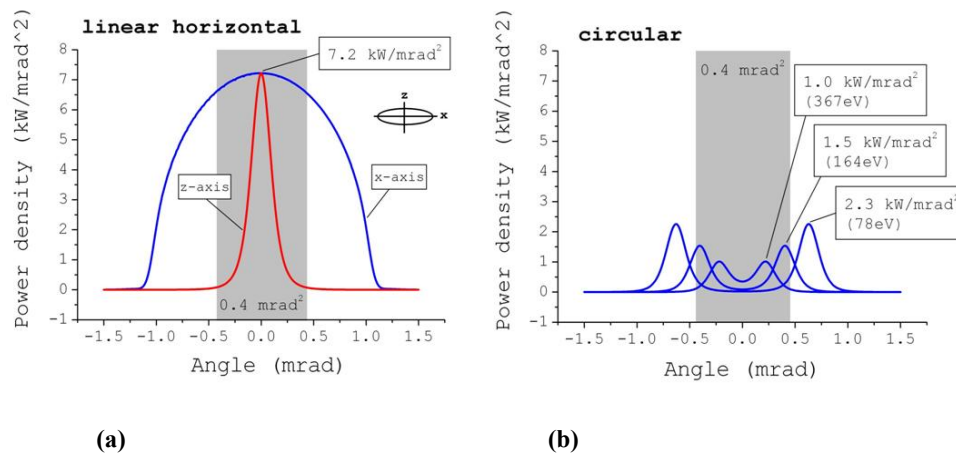


Figure 4: Power density emitted on the symmetry axis in linear-horizontal and circular polarization. The grey shaded area marks the movable white beam slits acceptance (0.4×0.4 mrad²).

For aligning the beamline, a beam profile with well defined boundaries in horizontal and vertical direction is needed. In linear polarization the shape is very wide and mostly cut by the aperture. The ring-shaped profile of the circularly polarized beam is equally sized in both directions and within the

aperture acceptance over a wide energy range, down to $\sim 200\text{eV}$ tuned energy (cf. Fig.4b).

Table 2. Total power emitted by HU71, for a beam current of 400 mA. Peak value of the angular power density and maximum total accepted power by the front-end (movable masks fully opened).

Current 400 mA	Total power (kW)	Peak power density (kW/mrad ²)	0.7 mrad ² FE acceptance (kW)	0.4 mrad ² FE acceptance (kW)
horizontal	3.10	7.19	1.25	0.67
vertical	1.81	4.79	0.94	0.49
circular	2.31	2.24	0.06	0.01

2 Optical layout of the beamline

The XMCD beamline is devoted to polarisation dependent, soft x-ray spectroscopy. Experimental techniques that will be implemented are mainly based on polarized x-ray absorption or scattering. This is in particular x-ray absorption spectroscopy (XAS), including x-ray magnetic circular/linear dichroism (XMCD/XMLD), resonant soft x-ray scattering (RSXS), and, as a potential future project, resonant inelastic x-ray scattering (RIXS).

The beamline is designed for a spectral range of 90-4000 eV, which starts at the Si $L_{2,3}$ absorption edges (99 eV), covering the $L_{2,3}$ edges of all 3d and 4d elements, as well as the $N_{4,5}$ and $M_{4,5}$ of the rare-earths and of U, and the K edges of C, N, O, F, P, S, Cl and K. The specified energy resolution is above $E/\Delta E = 5000\text{-}10000$ (FWHM) for most of the range (at least up to 2000 eV). The most frequently used energy range will be between 400 and 1500 eV, for which the performance of the optical components of the beamline is optimised.

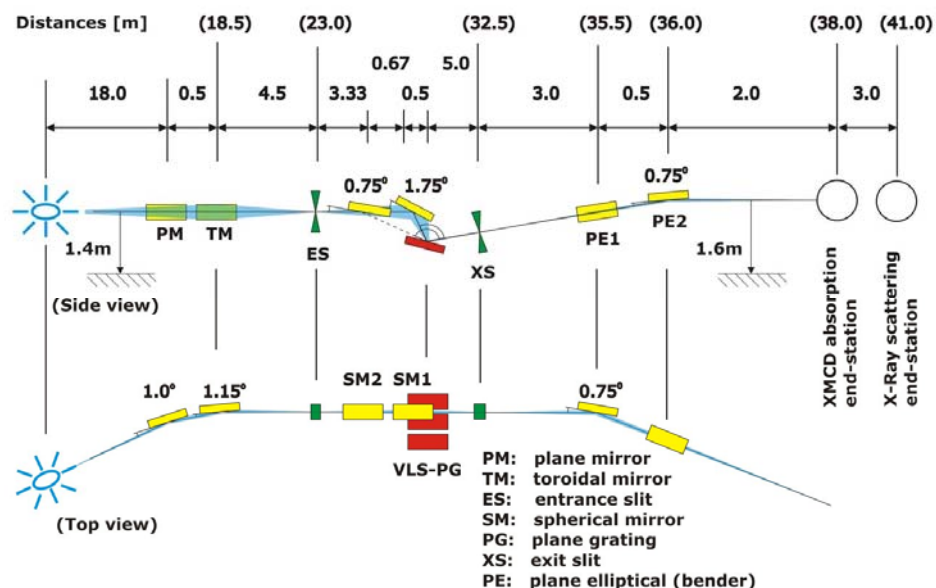


Figure 5: Schematic layout of the XMCD beamline.

The layout of the beamline can be subdivided in pre-optics section, monochromator section, including entrance and exit slits, refocussing section, and experiments section (including two in-line experimental stations), as outlined in Fig.5.

3 Pre-optics section

The pre-optics section includes a plane mirror (PM) and a toroidal mirror (TM). The plane mirror removes most of the unwanted radiation and heat load. The toroidal mirror focuses the x-ray beam vertically onto the entrance slit and horizontally onto a virtual plane, located 2m upstream the exit slit. Both mirrors are Au coated, and with a size of $400 \times 15 \text{ mm}^2$ (both) most of the beam delivered by the undulator is accepted, even at the lowest energies (big source size). The angles of incidence are 1° for PM and 1.15° for TM. These values have been chosen in order to trade-off between reflectivity of the Au coating at high energy (max 4000eV) and absorbed power (at gracing angles the power footprint on the mirror surface is enlarged and the power density reduced).

The vertical demagnification in the pre-optics section is about 4:1. In the monochromator section the vertical beam size is again slightly magnified due to the long exit arm (distance SM-XS). The (qualitative) beam size evolution along the beamline is shown in Fig.6. Ray-tracing simulations indicate that the vertical beamsize at the entrance slit will be of the order of $10 \mu\text{m}$ FWHM or less for energies above about 300eV (assuming meridional and sagittal slope errors of $1.5 \mu\text{rad}$ and $5 \mu\text{rad}$ RMS, respectively, for PM and TM). At lower energies the vertical beamsize can be considerably larger (up to about $60 \mu\text{m}$ FWHM at 70-100eV) due to higher source divergence.

Distances [m]									
d1	d2	d3	d4	d5	d6	d7	d8	d9	d10
18.0	0.5	4.5	4.0 (3.33)	0.5 (1.17)	5.0	3.0	0.5	2.0	3.0

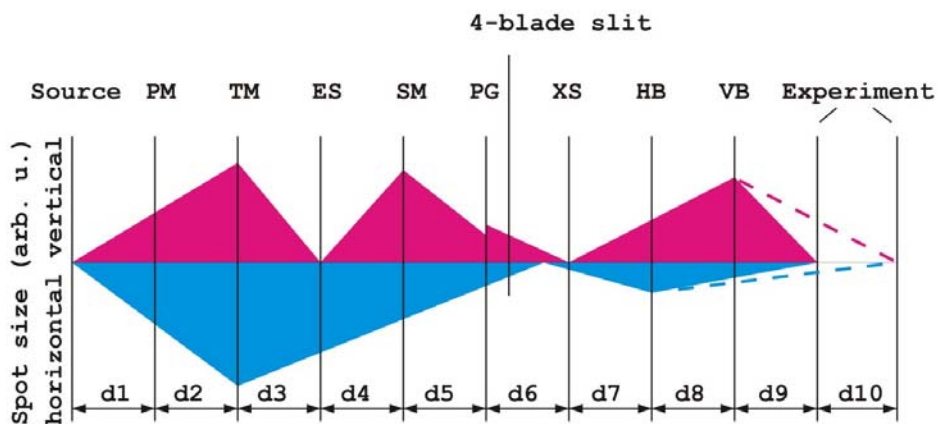


Figure 6: Horizontal and vertical beam size along the beamline (qualitatively).

4 Monochromator section

The beamline is designed with two different included-angles (fixed), variable line spacing plane grating monochromator (VLS-PGM), which includes an entrance slit (ES), two interchangeable spherical mirrors (SM1 and SM2) which define the include angles, followed by three interchangeable plane gratings (PG), and a fixed exit slit (XS).

This type of monochromator has the important advantage of being suitable for fast energy scans (50eV/min, "on-the-fly" scans), because the scanning mechanism is a simple rotation of the grating. Fast scanning is one way to minimize time drifts in x-ray magnetic circular dichroism experiments which produce dichroism artefacts. It will be the primary mode of operation of this monochromator. Secondly, the monochromator focuses diffracted and zero order light onto the exit slit plane (vertically) which can be used in coherent scattering experiments.

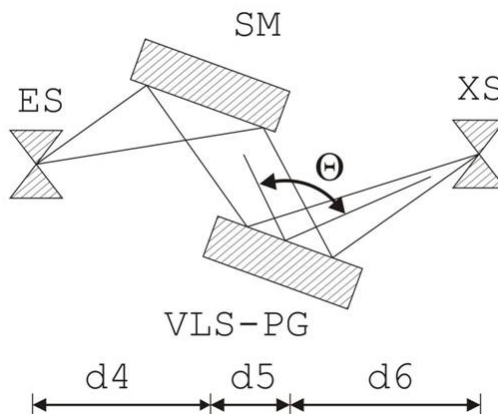


Figure 7: Layout of the VLS-PGM monochromator (side view): entrance slit (ES), spherical mirror (SM), VLS plane grating (VLS-PG), and exit slit (XS). The include angle Θ is fixed.

Finally, this monochromator is expected to provide high photon flux and good spectral resolution over an extended energy range. The XMCD beamline will cover the entire energy range with only three gratings, each of them with different line spacing, and two fixed included angles (defined by the two spherical mirrors SM1 and SM2).

Table 3. Geometrical parameters of the monochromator.

	Distance (m)
$d_{4,SM1}$	4
$d_{4,SM2}$	3.33
$d_{5,SM1}$	0.5
$d_{5,SM2}$	1.17
d_6	5

The geometry of the monochromator is outlined in Fig.7; the geometric parameters are defined in Table 3. The overall design of the monochromator constricted by a couple of constraints:

- 1) The available floor space allows a maximum monochromator length (from ES to XS) of 9.5m.
- 2) An exit arm (distance between the grating and the XS) of about 5m appears to be a good trade-off between mechanical requirements (resolution and stability of the grating pitch rotation) and $E/\Delta E = 5000-10000$ energy resolution over a wide energy range, at reasonable vertical exit slit opening (15 μm has been chosen for standard operation).
- 3) In order to have the best demagnification by the spherical mirrors SM1 and SM2, under the constraints 1) and 2), the mirrors will be located as close as possible to the gratings.
- 4) Due to VLS technology the spectral defocussing in the exit slit plane is almost compensated, thus enabling energy scans at fixed exit slit position with negligible degradation of the energy resolution.

In the following we give a detailed description of the different components of the monochromator.

The entrance slit (ES) is located in the vertical focus of the toroidal mirror TM. It cuts the tails of the beam which are due to aberrations of the toroidal mirror, and can be considered as the virtual source of the monochromator. In case of a heat bump on the optical surface of PM and TM, the increased beam spot will be cut by the entrance slit, thus reducing the intensity of the virtual source. This effect is partly compensated by the higher flux of the source, as it affects mostly the low energy range. Moreover, the use of a monochromator with entrance slit ensures better stability, as fluctuations of the vertical beam position will result in intensity fluctuations, without major effects on the energy resolution and calibration of the beamline. In practice, for energies above about 300eV the entrance slit width will have only very little influence on the total energy resolution of the monochromator, which is mainly determined by the slope error of its optical elements and by the width of the exit slit. At energies below 300eV the target energy resolution of $E/\Delta E = 5000-10000$ can be achieved by setting the entrance slit to $\sim 15\mu\text{m}$. In case of experiments requiring this high resolving power at low energies only a part of the flux transmitted by the pre-optics will be usable. So, in general the entrance slit opening can be kept at 15 μm for the whole energy range 90-4000eV.

At a distance $d_{4,SM1} = 4\text{m}$ ($d_{4,SM2} = 3.33\text{m}$) behind the ES, the spherical mirror (SM1 or SM2) reflects the beam downwards onto the grating (cf. Fig.7) The angles of incidence are $\theta_{SM1} = 1.75^\circ$ and $\theta_{SM2} = 0.75^\circ$. These mirrors have the double function of refocusing the beam vertically onto the exit slit (XS) and defining the include angle of the monochromator of 175° and 177° , respectively. These mirrors are kept at fixed deflecting angles. They are both Au coated and their size is $200 \times 10\text{mm}^2$ (meridional \times sagittal).

At a distance $d_{5,SM1} = 0.5\text{m}$ ($d_{5,SM2} = 1.17\text{m}$) downstream SM1 (SM2), the plane VLS gratings are the diffractive elements of the monochromator (see Fig.7). Three different gratings have been chosen in order to cover the whole energy range of the beamline. The whole energy range is divided into low-energy

(LE), medium-energy (ME) and high-energy (HE), the the gratings are assigned accordingly. The choice of the variable line spacing ensures proper focusing of almost all wavelengths diffracted in the 1st inner order, i.e. the exit slit can be kept almost always at the same position (the focal distance varies only a few mm in total). Moreover the VLS gratings efficiently correct the aberrations of the spherical mirrors in order to minimise the beamsizes on the exit slit.

Table 4. Working energy ranges and groove density parameters of the gratings.

	$\Theta = 175^\circ$ (eV)	$\Theta = 177^\circ$ (eV)	D_0 (lines/mm)	D_1 (lines/mm ²)	D_2 (lines/mm ³)
LE	80-300	250-500	200 ($\pm 0.25\%$)	0.080 ($\pm 0.25\%$)	$0.24 \cdot 10^{-4}$ ($\pm 4\%$)
ME	350-1500	1300-3000	800 ($\pm 0.12\%$)	0.320 ($\pm 0.20\%$)	$0.96 \cdot 10^{-4}$ ($\pm 10\%$)
HE	600-2000	2000-4000	1200 ($\pm 0.15\%$)	0.479 ($\pm 0.2\%$)	$1.44 \cdot 10^{-4}$ ($\pm 7\%$)

The groove density of the VLS gratings is defined by $D(y) = D_0 + D_1 \cdot y + D_2 \cdot y^2$, where y is the longitudinal coordinate (along the beam propagation direction), D_0 the groove density in the centre of the grating ($y = 0$), and D_1 and D_2 the of the linear and quadratic variation coefficients of the groove density. The three gratings have been chosen according to the general requirement for $E/\Delta E = 5000$ - 10000 energy resolution at $15\mu\text{m}$ exit slit opening, wide operational energy range, and high flux. However, in the optimisation procedure the energy range 400 - 1500eV has been given higher priority.

In the following, we give more detailed information on the gratings (cf. Table 4).

- 1) The HE grating is designed for an energy range up to 4000eV (at 177° include angle) with a reasonable trade-off between energy resolution and flux. With $D_0 = 1200\text{lines/mm}$, D_1 is optimised for energies around 1000eV . A blazed groove profile, with 0.6° blaze angle gives best throughput at high energies (3 - 4keV), where the undulator flux is considerably reduced. The same values provide a good higher harmonics rejection in the energy range 600 - 2000eV , where the grating will work at 175° fixed included angle (SM1).
- 2) The ME grating is chosen to cover the energy range 400 - 1500eV , exhibiting reasonable energy resolution by using one grating and one include angle (175° and SM1), which permits a broad range of experiments without changing the grating. The grating is foreseen with $D_0 = 800\text{lines/mm}$, and D_1 is optimised at 700eV . The groove profile can be either blazed (with 0.6° blaze angle) or laminar (with 10nm groove depth). In combination with SM2 the same ME grating can also be used to cover the energy range 1300 - 3000eV . However, in this energy range a blazed profile is clearly necessary in order to have an acceptable diffraction efficiency in the 1st internal order;

3) The LE grating is designed to cover the low energy range (90-400eV). It was chosen to maximise the energy resolution around the rare-earths $N_{4,5}$ absorption edges ($\sim 150\text{eV}$), with the condition that the grating can still reach the minimum energy of 80-90eV. With a groove density of 200lines/mm, the requirements are fulfilled in combination with SM1 for the energy range 80-300eV and SM2 for energies above 250eV. The groove profile is laminar, with 35nm groove depth. This choice of grating is imposed by the large included angles which are necessary for the higher energies.

Because of the different energy ranges all gratings are Au coated, although different types of coating might be better suited for the high energies (Ni, for example, would be better than Au between 2 and 3keV, but worse at higher energies). Figure 8 shows the diffraction efficiency of the various gratings calculated with the software REFLECT [3].

The exit slit XS determines the spectral resolution of the monochromator. As mentioned above, the monochromator is designed for $E/\Delta E = 5000-10000$ spectral resolution in a wide energy range, and with $15\mu\text{m}$ vertical exit slit opening. This slit opening should be sufficiently large as to allow stable operation of the monochromator at high energy resolution, even with the foreseen fast energy scans. However, for a large number of experiments the energy resolution can be relaxed to work with wider vertical XS slit opening. Still, if higher energy resolution is required (as for example might be the case in RIXS experiments), enough margin is left to close XS below $15\mu\text{m}$.

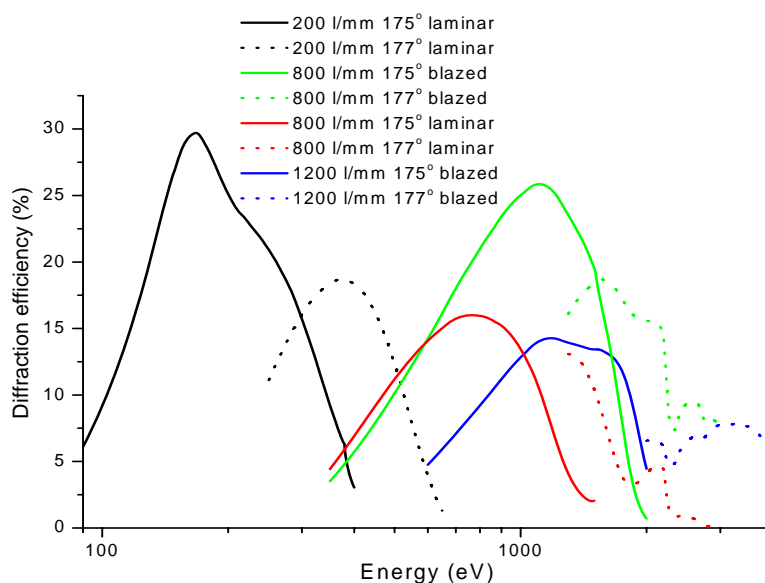


Figure 8: Diffraction efficiency of the different gratings (Au coated).

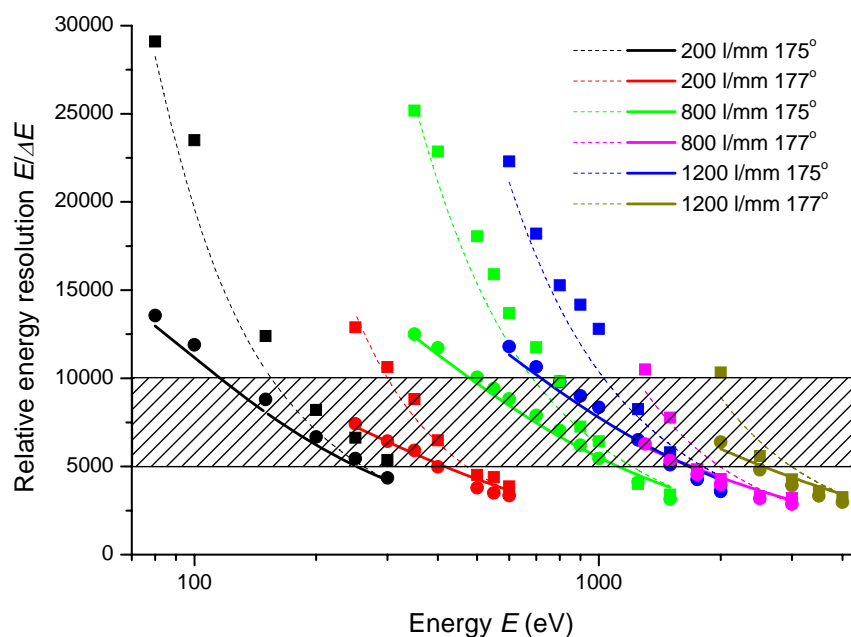


Figure 9: Relative energy resolution of the different gratings, calculated analytically (lines) and by ray-tracing simulation (symbols).

The expected energy resolution of this monochromator has been calculated both, analytically and by ray-tracing. The best case, i.e. smallest possible beamsize at the XS for each energy, and XS opening of $5\mu\text{m}$ (dotted lines for the analytical model and full squares for the ray-tracing), and for the case of $15\mu\text{m}$ XS opening (continuous lines for the analytical model and full circles for the ray-tracing) are shown in Fig.9. The exit slits are kept at the same position (i.e. at the same distance d_6 from the gratings) for all energies. Meridional and sagittal slope errors for both, the spherical mirrors and the gratings, are assumed of 0.5 and $5\mu\text{rad}$ RMS, respectively. The energy resolution of the monochromator is affected mainly by the meridional slope errors of both gratings (σ_{GR}) and mirrors (σ_{MI}) and by the opening of the XS, while the vertical width of the ES (σ_{ES}) is important only at energies below 250-300eV. The beam size at the exit slit (Δz_{XSreal}) can be calculated from the beamsize at the entrance slit (Δz_{ES}), considering the "defocusing" effect of the slope errors of both mirror (Δz_{MI}) and grating (Δz_{GR}). For our monochromator this is given by

$$\Delta z_{XSideal} = \Delta z_{ES} \cdot \frac{d_5 + d_6}{d_4 \cdot c_{ff}},$$

$$\Delta z_{GR} = \left(1 + \frac{1}{c_{ff}}\right) \cdot d_6 \cdot \sigma_{GR},$$

$$\Delta z_{MI} = 2 \cdot \frac{d_5 + d_6}{c_{ff}} \cdot \sigma_{MI},$$

with $c_{ff} = \frac{\cos \beta}{\cos \alpha}$, and α , β are the incidence and diffraction angles of the grating, with respect to the surface normal. Combining these equations, we can determine the real beamsize at the XS as:

$$\Delta z_{XSreal} = \sqrt{(\Delta z_{XSideal})^2 + (\Delta z_{GR})^2 + (\Delta z_{MI})^2}.$$

The energy resolution corresponding to this beamsize follows then easily by differentiating the grating equation $\sin \alpha + \sin \beta = D_0 m \lambda$, where $m = 1$ for the 1st diffraction order of the grating and λ is the wavelength:

$$\frac{E}{\Delta E} = \frac{\lambda}{\Delta \lambda} = \frac{D_0 m \lambda}{\cos \beta} \cdot \frac{d_6}{\Delta z_{XSreal}}.$$

The contributions from the different terms depends on the tuned energy of the radiation before the monochromator. In general, Δz_{GR} increases less with energy than $\Delta z_{XSideal}$ and Δz_{MI} . Thus, in the low energy side of the working range of a given grating Δz_{GR} is the dominating contribution to $E/\Delta E$, while on the high energy side all three terms are comparable. In general it will therefore be crucial that the meridional slope errors of both the gratings and the spherical mirrors can be kept to values of the order of 0.5 μ rad RMS or better.

5 Refocusing section

Refocusing after the exit slit is done in both, horizontal and vertical directions by a Kirkpatrick-Baez (KB) set of plane-elliptical bendable mirrors. This solution allows to focus the beam in either experimental station, but also to collimate the beam which results in a lower flux density on the sample. Depending on the application and the type of experiment, the flexibility to focus the beam (approx. $100 \times 10 \mu\text{m}^2$), or widen it (up to $1 \times 1 \text{mm}^2$) is very convenient. The latter case is useful for all applications requiring full flux but low flux density, e.g. sensitive samples, like molecules or organic magnets.

As the monochromator is quite long, limited space is available for the refocusing section (roughly 9m for both, refocusing and experimental sections). This limits the beam size (demagnification) in the experimental stations. In order to fully exploit the small source size in vertical direction, the horizontally refocusing mirror (PE1) will be placed downstream before the vertically refocusing mirror (PE2), located 3m and 3.5m behind the exit slit, respectively. The first experimental station is located 2m downstream PE2 (however, 1.5m should also be feasible if necessary), while the second experimental station is at 5m (but 4m should be feasible as well). The vertical beamsize in the experimental stations depends essentially on the size of the monochromatic beam at the XS, while the XS opening has only a minor influence. The meridional slope error of the PE2 is crucial for the smallest spot size possible. Assuming 1 μ rad slope error, the vertical spotsize is around 10 μ m in the first experimental station, and about 25 μ m in the second station over most of the energy range. Reducing the meridional slope error to 0.5 μ rad (PE2) it should be possible to have 5-6 μ m vertical beamsize in the first experimental station, which might be useful for RIXS experiments. Therefore, the experimental chamber which is more likely to host in the future a RIXS spectrometer should be located closely to PE2. The horizontal beamsize is less affected by the meridional slope error of PE1 because of the larger horizontal

source size. Typically the beam should have a horizontal size of $\sim 100\mu\text{m}$ at the first station and $\sim 250\mu\text{m}$ at the second, for most energies.

Both mirrors are Au coated and will be set to 0.75° grazing incidence, which ensures high throughput up to the highest energies (4000 eV). The proposed size is $300\times 15\text{mm}^2$ (meridional \times sagittal) for PE1 and $400\times 5\text{mm}^2$ for the PE2, in order to accept the full beam in the whole energy range.

6 Experiments section

The beamline feeds two UHV compatible experimental stations. A chamber for absorption experiments, including x-ray magnetic circular/linear dichroism, and a chamber for resonant x-ray scattering experiments. The experimental chambers are positioned in-line for simplicity.

The design of both experimental chambers is yet at an early stage, and detailed discussion of their characteristics is beyond the scope of this report. The main feature of the absorption chamber is a superconducting magnet for magnetic fields up to $\sim 7\text{T}$ and XMCD/XMLD experiments, in the temperature range 2-300K. The scattering chamber will have a versatile UHV-compatible diffractometer, with a 0.1-0.5 T electromagnet with versatile field orientation. The chamber should also give the possibility to perform XMCD experiments with moderate magnetic fields, and shall be equipped with a sample cooling stage. Moreover, a possible future extension will be to equip one of the two chambers with a RIXS spectrometer.

7 Power load on the optical elements

The undulator source reaches the maximum emitted power in linear horizontal polarization at high magnetic fields, i.e., at a small gap which means at low photon energies. In this tune most of the unwanted power at higher harmonics is emitted off-axis and can be removed by selecting an appropriate aperture. The optimal trade-off between power and tuned flux can be estimated by a calculation of the emitted flux and power of the first harmonics, with the aperture opening as parameter (Fig. 10).

At the limits of the power footprint a steep temperature gradient induces significant slope errors. In order to avoid the latter to affect the performance of the beamline, the limits of the power footprint are to be kept away from the flux footprint which implies a larger acceptance than the one given by the source size and divergence. Thus, especially the first optical elements have to withstand substantial heatload for good optical performance. Besides the total power load, the peak power density can also be quite significant at small undulator gaps. Especially at the first optical elements the heat induced bump due to high power density locally increases the slope error and requires effective cooling in order to maintain the optical performance. Again, the most critical situation occurs at low energy and linear-horizontal polarization. An example of the energy dependence of the incident and absorbed power and peak power density is given for the case of PM in Figure 11.

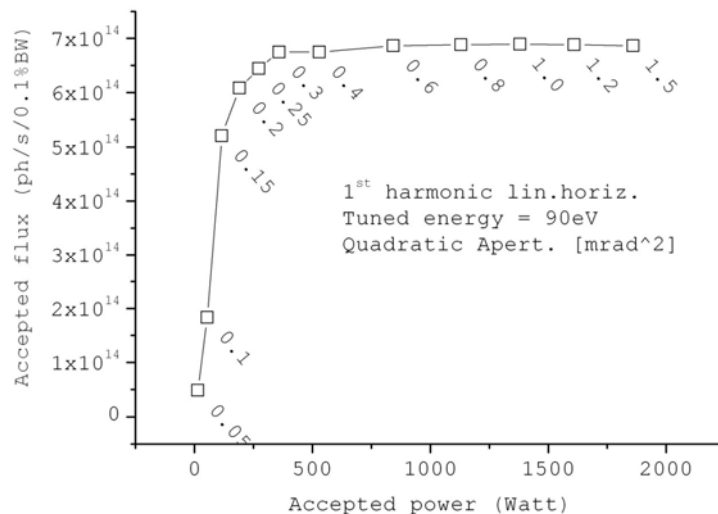


Figure 10: Trade-off between accepted flux and accepted power from the 1st harmonic at linear-horizontal polarization through different (quadratic) apertures (400 mA beam current). The labels indicate the full size slit acceptance [4].

The first optical element is a vertical plane mirror (surface normal in the horizontal plane) which removes most of the unwanted heat load. The second element is a toroidal mirror with sagittal focussing in vertical direction. Although the mirror is under substantial heat load, heat induced aberrations are less critical in vertical direction because of the sagittal forgiveness factor. For the spherical fixed included angle mirrors, although meridionally focussing, the power density is not very high and heat induced slope errors should be easily kept low with side cooling. The power load on the grating is not very high. Still, cooling has to be considered as the power load affects spectral resolution. A rough estimation of power load and power density can be easily obtained by taking the grating as a gold coated mirror. When used as diffracting devices, the highest power load delivered to the gratings is at the least grazing angle (87.9°), which is the case for the LE-grating at 175° fixed included angle. Downstream the exit slit the total power is reduced considerably and the power absorption of the following optical elements even in the worst case should not exceed 2 W. However, with the grating at zero-order position (acting as a mirror) which is of interest for coherent scattering with pink beam the heat load beyond the grating has to be taken into consideration.

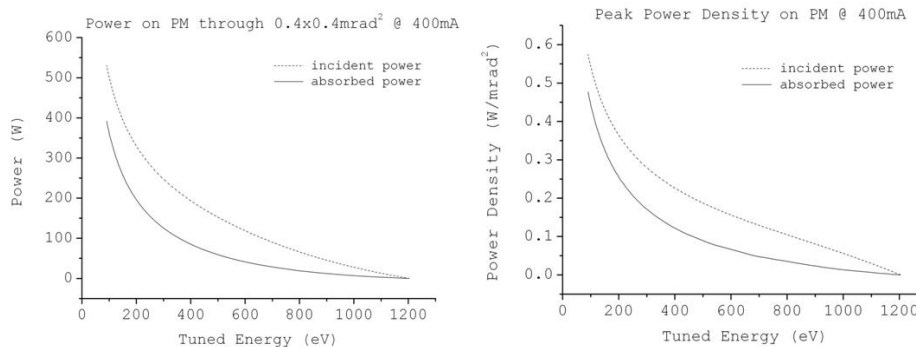


Figure 11: Total power and peak power density absorbed by the first mirror (PM).

The power load absorbed by the optical elements has been determined by spectral power calculations, taking into account the reflectivity of the mirrors (Au coated) and the angle of incidence [1], with the undulator at minimum gap (79eV). Further on we assumed linear horizontal polarization, 400 mA ring current, fully opened slits (fully closed for the load on the slits) and steepest angle of incidence as the worst case scenario.

Table 5: Absorbed power, maximum power density, angle of incidence of the beam, suggested material and cooling scheme for the various optical elements of the XMCD beamline (at minimum gap and the grating in zero order position).

Optical Element	Abs. (W)	Trans. (W)	Max. power density (W/mm ²)	Inc. angle (grazing)	Suggested material	Suggested cooling
WBS (0.4x0.4mrad)		651				
PM	522	129	0.33	1°	Glidcop	internal
TM	65	64	0.031	1.15°	Si	side
ES	0.. 64	64	792	90°	MO, W	side
SM (1.75°)	37	28	0.043	1.75°	Si	side
SM (0.75°)	15	39	0.07	0.75°	Si	side
PG 1.75°	19 (33)	9 (16)	0.031	2.1°	Si	side
XS	0.9 (16)	9 (16)	>1000	90°	Mo, W	side
PE1	2 (4)	7 (12)	0.0047	0.75°	Si	non
PE2	1 (2)	6 (10)	0.0044	0.75°	Si	non

The main power load is absorbed by the first mirror. The first mirror should be cooled internally as most of the power load is concentrated on a small region. A set of small channels behind the surface works well in case of a molybdenum substrate (positive test results at Elettra). The mirrors inside the monochromator (silicon substrate), i.e. the spherical mirrors which define the fixed include angle, should have side cooling and laminar cooling fluid flow (if possible). For the grating the most adopted solution is the use of copper braids, i. e. direct side cooling with a water circuit. The cooling pipes move together with the gratings when exchanged under vacuum. The heat load on the optical elements and suggested cooling is summarized in Table 5. The most critical element is the grating which absorbs a heat load of up to 19W if we restrict zero-order beam to 175° include angle.

8 Diagnostics system

Several types of devices for photon beam monitoring along the XMCD beamline are to be installed. Some of them are offline, that means they cannot be used during data collection, and some other are online devices, that is they can be used during data collection. A brief description of each of these components is given below.

Multilayer screen

It consists of a cooled multilayer mirror deflecting the undulator radiation by 90° onto a phosphor-coated view port, where the optically visible beam footprint is recorded with a CCD camera. Therefore, even being illuminated by the white beam, the multilayer reflects a limited band of energies, in such a way that a much narrower spot size, fully transmitted by the front end can be used for monitoring the photon beam position. This is an offline diagnostics device.

X-ray beam position monitor

X-ray beam position monitor (xBPM, BESSY II or similar design; see K. Holldack et al., AIP conference proceedings 521, 354 (2001)): It consists of a two-dimensional blade monitor with four insulated tungsten or molybdenum blades mounted at an angle of, e. g., 45° each with respect to the vertical direction inside a photon beam opening within a cooled OFHC copper block. Blade angles and distances are optimized according to spectral and angular characteristics of undulator as well as with respect to parasitic dipole radiation. The readout of photocurrent is done using a four-channel electrometer including negative bias voltage on the tungsten blades. This is an online diagnostic system.

Beam diagnostics set-up

The beam diagnostics set-up: consists of a six-way cross with a linear feedthrough including fluorescent screen and an isolated high-transmission tungsten mesh for the white beam section, or gold mesh for the monochromatic beam section. The fluorescent screen and the mesh are fully retractable from the photon beam path. The high-transmission mesh is an online diagnostic device, whereas the fluorescence screen is not.

Beam monitor

The beam monitor consists of a six-way cross with a linear feedthrough which includes a thin film metal sample that partially intercepts the monochromatic beam. The drain current is measured in order to monitor the selected photon energy and polarization during data collection. This is an online diagnostic system.

Gas cell

In order to calibrate the spectral resolution of the monochromator a gas cell will be included in the monochromatic section of the beamline. The gas cell

consists of a 6-way cross including a cylindrical gas ionization chamber, a leak valve and a channeltron detector. Both the beam entrance and exit ports include one pair of aperture disks each, with small beam orifice for differential pumping between aperture disks. Alternatively, window gate valves with thin Al windows may be used instead of the differentially pumped orifices. This is an offline diagnostic system.

I_0 monitor chamber

This is a small vacuum chamber that includes a rotary feedthrough with a fluorescent screen and a high-transmission gold mesh, and a photodiode. The mesh arrangement includes a drain current set-up (BNC feedthrough, UHV-compatible Kapton-insulated coaxial cable). In addition a gold evaporator is installed inside the vacuum chamber for deposition of fresh gold layers on the gold mesh.

Beam diagnostics included in the entrance and exit slit set-ups

The entrance and exit slit set-ups will also include some diagnostics consisting on a two-jaw horizontal aperture upstream the slit blades. The aperture jaws will be electrically isolated with respect to ground and will include a drain current set-up. The entrance slit blades themselves will serve as online beam diagnostic devices by measuring photon beam-induced differential drain current from the slit blades. Downstream both the entrance and the exit slit setup (but still within the same setup, if possible) a retractable gold or tungsten mesh shall be installed for measuring the relative transmission through the corresponding slit via the mesh drain current.

Layout of the beam diagnostics

Some parts of the beamline, like the space between PM and TM or that between SM1/2 and the VLS gratings, cannot be accessed because adjacent optical elements will be installed in the same chamber. A suggested layout of beamline components and diagnostic devices is shown in Fig. 12.

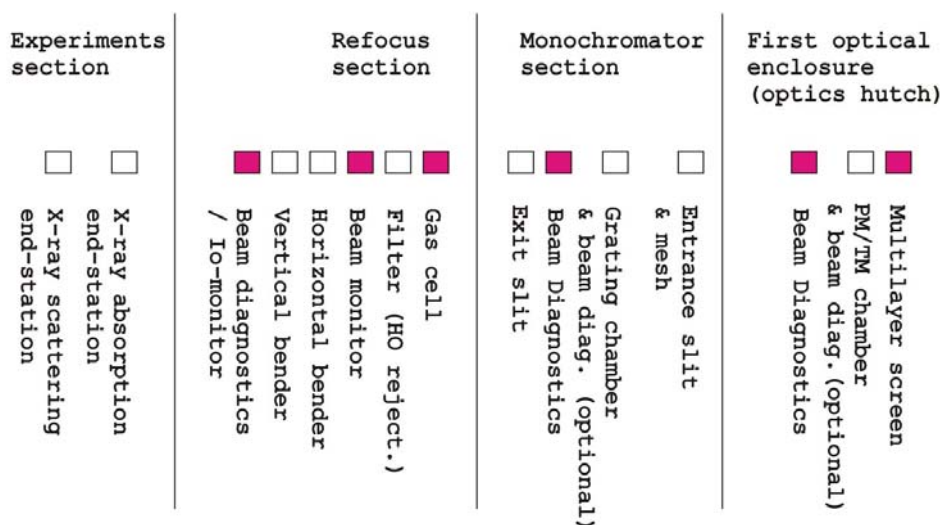


Figure 12: Layout of the beamline components, including the suggested diagnostic units.

References

- [1] D. Einfeld, E. Al-Dmour, J. Campmany, M. Munoz, F. Perez, and M. Pont, *AAD-SR-AR-0042*
- [2] SPECTRA7.2 code from SPring8
- [3] REFLECT code from BESSY
- [4] XOP2.11 code from ESRF